Sputtering of Single Crystals: Experimental Evidence of the Ejection Process

By Nicholas Winograd
Department of Chemistry, Penn State University
152 Davey Laboratory, University Park, PA 16802, USA

Synopsis

The objective of this review is to summarize recent experimental evidence of the sputtering of atoms from single crystal targets. The information is extracted primarily from literature published within the last 10 years and is meant to compliment other recent reviews on single crystal sputtering. The emphasis of the discussion is on experiments that are performed on well characterized surfaces obtained under low-dose conditions. Because of this restriction, most of the experiments utilized laser postionization as the detection scheme. The discussion of experimental results is focused mainly toward comparison with results of molecular dynamics computer similations. The review includes a discussion of experimental techniques, a sampling of results obtained at normal incidence with keV Ar^+ ions, and others obtained at variable incident angles. In addition, energy and angular distributions of ground-state and excited-state sputtered atoms are compared in detail.

1 Introduction

Results of experimental studies of single crystals bombarded by keV particles offer a unique perspective on the fundamental processes underlying the scattering events associated with atom ejection. Since Wehner (1955) first observed his anisotropic emission - his famous 'spots' - there has been a lot of spirited discussion about the mechanisms of energy dissipation, particularly with regard to validating proposed theories. While in the early years single crystal sputtering was mainly of interest for its theoretical significance, later, single crystal effects became important in characterization of surface structure. Throughout this period, we have seen enormous advances in experimental technique and in the ability to quantitatively predict detailed information about the trajectories of ejected species. In this chapter, we review some of the important early studies and detail the recent strides

in laboratory techniques which have helped to reveal experimental evidence for ejection processes associated with single crystal targets.

2 Historical Perspectives

The earliest systematic studies of the sputtering of single crystals date to 1955 and the pioneering work of Wehner (1955). These studies showed that W atoms ejected from single-crystal W targets bombarded by 150 eV Hg^+ ions left the surface along preferred crystallographic directions. This anisotropy was in direct contradiction to many early theories of sputtering which suggested that the process was dominated by a thermal process or by sublimation (Von Hippel, 1926 and Townes, 1944) which would exhibit a yield with a cosine-like angular dependence. Wehner had convinced his peers by his use of single crystals that momentum transfer played a key role in the phenomenon.

During the 1960's many studies ensued which examined issues such as mass dependence, energy dependence and crystal face dependence of the sputtering yield. A few key observations emerged from many elegant experiments. For the fcc metals, for example, it was found that the preferred ejection generally occurs along the <110> bulk crystal direction (Anderson & Wehner, 1960). Single crystal effects were also observed for hcp and bcc metals (Nelson, 1963; Robinson & Southern, 1968). Interestingly, semiconductor crystals appeared much less anisotropic than metals (Southern et al., 1963). The reason for this early erroneous conclusion was primarily the more extensive damage suffered by these materials from the bombardment process.

Single crystal sputtering during the early period provided critical information for the theoreticians. As noted above, the evaporation models had to be discarded. An initial explanation of the anisotropies came from Silsbee (1957) who suggested that momentum could be focused along a row of equally spaced spheres if the distance between centers is less than twice the atomic diameter. This proposal inspired much more thinking about the problem from an atomic point of view. As the story goes, Wehner attempted to look for these Silsbee chains by constructing a model of a crystal with balls attached by strings to the ceiling. He then struck this crystal with a primary particle (ball) and photographed the event with a strobe lamp. The results were inconclusive but representative of how clever Wehner (1992) could be.

Computer simulations offered new hope to understanding single crystal sputtering. The modeling could be performed on a realistic crystallite since the lattice positions were known. Reasonable interaction potentials were becoming available in the mid-1960's and it was possible to solve Newton's equation of motion for a

collection of atoms subject to an initial particle bombardment. Ironically, some of the early modeling studies supported the conclusions of Silsbee (Gibson et al., 1960). The calculations clearly revealed that focused collision sequences could contribute to sputtering. An early pioneer in computer modeling, Don Harrison, found that focused collision sequences were possible, but in fact were quite rare (Harrison et al., 1966, 1968). More importantly, he suggested that the sputtering event was dominated by near-surface collisions involving just the first couple of layers of the solid. We will discuss the significance of this important statement in later sections. Lehmann and Sigmund (1966) later also proposed that the surface structure dominated the angular distributions. They noted that when subsurface atoms attain a kinetic energy on the order of the surface binding energy, only head-on collisions can lead to emission of surface atoms. They also noted that subsurface atoms could be ejected through potential minima in the surface layer, created by gaps between atoms. These alternative explanations of the angular anisotropies helped to explain a number of problems with the focused collision sequence models associated with hcp crystals (Hofer, 1973). More importantly, however, they suggested that in order to establish a quantitative understanding of single-crystal sputtering, it would be essential for experimental data to be obtained from crystals with well-characterized surfaces.

There was much controversy about these ideas that broiled all the way through the 1970's. As knowledge of handling single crystals improved, experimental methods which required a lower dose of incident ions were presented. For example, Szymczak and Wittmaack (1980) developed a sensitive detection scheme for gold using Rutherford backscattering to analyze material collected on a plate. They concluded that for such high-Z metals as gold it might be necessary to include deep-layer focusing to explain the large anisotropies they observed. Hundreds of other articles on single crystal sputtering appeared during that time. Most of these have been thoroughly reviewed by Hofer (1991). He also provides a comprehensive list of important recent review articles. Most of this research effort produced a qualitative understanding of single crystal sputtering. For metals bombarded near normal incidence with keV heavy particles, the highest emission intensity is observed along open crystallographic directions in the plane of the surface. Other peaks may be observed in directions where it is easy for second-layer particles to escape. It was realized that a high bombardment dose could produce topographical features (Hauffe, 1991) that could lead to erroneous results. Moreover, surface cleanliness became an issue because of the proposal by Harrison, Lehmann and Sigmund that the sputtering mechanism involved mainly surface layers and hence would be influenced by adsorbed impurities. Energy distributions from single crystals were found to be qualitatively similar to those found from polycrystalline surfaces, although the peak in the energy distribution may not be the same as for

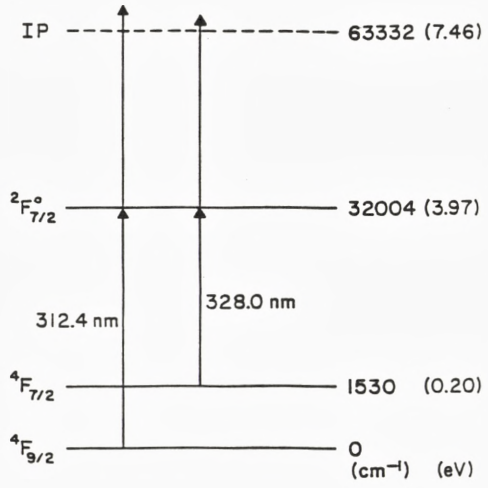

Figure 1. Partial energy level diagram for Rh. Ground-state Rh can be multiphoton ionized using two 312.4-nm photons. The first excited state can be probed by ionizing with two 328.0-nm photons.

amorphous systems and there may be structure in the distributions associated with direct recoils. (Reid et al., 1976)

More quantitative understanding of single crystal sputtering has been hampered by a number of factors. First, experimental techniques have not been generally available to examine bombarded single crystals at doses low enough ($<10^{14}$ ions/cm^2) to avoid artifacts. Secondly, the sputtering community has been slow to incorporate auxiliary surface characterization techniques such as low energy electron diffraction (LEED) and Auger electron spectroscopy (AES) into their apparatus. These methods show that the damage in single crystals is not removed unless the crystals are annealed well above their Debye temperature (Jenkins & Chung, 1971). Moreover, they show that even 'inert' metals such as copper and gold cannot be kept clean unless the vacuum is reduced to the 10^{-10} torr regime. Unless single crystal surfaces are prepared according to the rigors of modern surface physics, it is not possible to be sure that the resulting measurements can quantitatively be compared to proposed models and that data can even be quantitatively reproduced from lab to lab.

In this review, we examine the present status of experimental approaches to examining single-crystal sputtering. In general, the discussion will be restricted to experimental results obtained on well-characterized single crystal substrates obtained under low-dose conditions. The emphasis will be to present a limited data

base, primarily from our own laboratory, where quantitative comparison to theory is possible. It is hoped that this review will not only encourage more experiments, but that the theory, now dominated by computationally intensive molecular dynamics calculations, can be reinvigorated with new analytical approaches.

3 Experimental Techniques

To fully characterize the sputtering event associated with single crystals, it is desirable to be able to vary the angle of incidence of the primary particle and to detect in a state-selective manner the sputtered flux with energy, angle and mass selection. It is also critical to obtain such data without damaging the crystal surface. During the 1970's there were many attempts to get at this problem. One idea involves postionization of the ejected species either by electron bombardment (Lundquist, 1978) or by a low energy plasma discharge (Oechsner & Gerhard, 1972). The ion which is formed is then detectable within single particle detection limits using a mass spectrometer. The work of Thompson and his group (1963, 1978) also stimulated much interest in the time-of-flight (TOF) technique. In general, these methods require an incident dose of more than 10^{17} particles/cm^2, at least 3 orders of magnitude beyond the damage threshold. Another approach involved the excitation of ejected atoms by a laser, followed by the measurement of the doppler-shifted fluorescent intensity (Hammer et al., 1976). This scheme allows individual electronic states to be detected. Unfortunately, the fluorescence techniques have not yet been systematically applied to angular distribution measurements and they require beam doses well in excess of 10^{16} particles/cm^2. Finally, an elegant experiment has been devised to collect a small amount of metal sputtered onto a detector using Rutherford backscattering spectroscopy (Szymczak & Wittmaack, 1980). Here, the dose could be kept in the range of 10^{15} particles/cm^2.

During the 1980's new laser techniques emerged which exhibited the necessary characteristics needed for efficient postionization. These include multiphoton resonance ionization (MPRI) (Winograd et al., 1982; Hurst & Payne, 1988), multiphoton nonresonance ionization (Becker & Gillen, 1984), and single-photon ionization (Schuhle et al., 1988). The MPRI method seems best from the point of view of maximizing sensitivity and state selection as pointed out by Hurst et al., (1979). Other schemes may prove viable as well in the future, although none have yet been applied to the study of the sputtering of single crystals. The MPRI approach for atoms can be employed by inspection of the electronic energy level diagram shown in Figure 1 for Rh, which will be used as a model system. There are a variety of electronic states that can be directly probed by an appropriate choice of the ionization wavelength. For example, the $^4F_{9/2}$ ground state can be ionized through

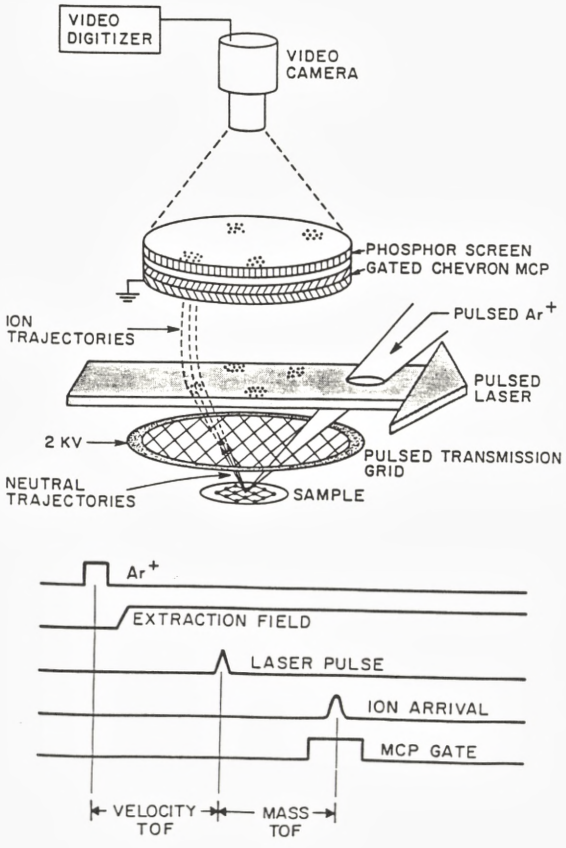

Figure 2. Detector for performing energy and angle-resolved measurements of neutral species desorbed from surfaces, along with the appropriate pulse sequences.

the $^2F_{7/2}$ state with two 312.4-nm photons. The $^4F_{7/2}$, $^4F_{5/2}$, and $^4F_{3/2}$ states lie within 1 eV of the ground state and can be ionized with two photons of slightly different energy (Moore, 1971). For this system $^4F_{9/2} \leftarrow {}^4F_{7/2}$ in the gas phase is a forbidden transition, so it is possible to make detailed measurements on both states and to directly compare the results.

The experimental geometry for such a scheme is shown in Figure 2 (Winograd et al., 1986). A pulsed ion beam of 200 ns serves to generate a burst of desorbed particles localized in space moving away from the target surface. At an appropriate time, a laser pulse tuned to an atomic resonance of the emitted particle is directed a few millimeters above and parallel to the target. As discussed by others (Hurst

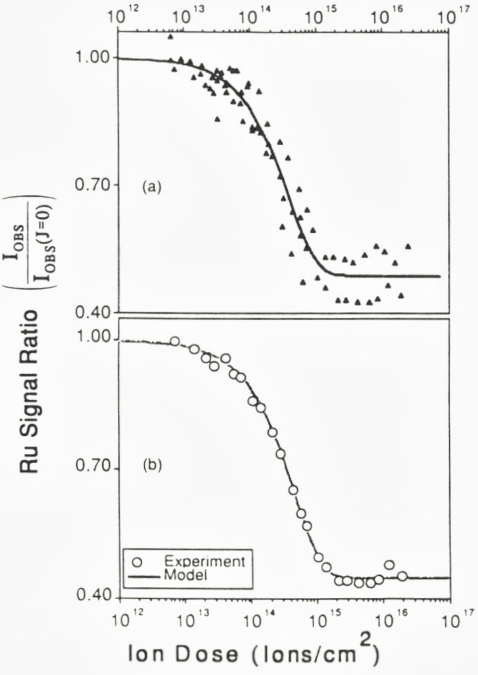

Figure 3. The Ru SNMS signal ratio, $I_{\rm obs}(J)/I_{\rm obs}(J=0)$, from the Ru(0001) surface plotted as a function of primary-ion dose, J. Results from four separate experiments are shown in (a) while results from a single experiment are shown in (b). The solid lines are the result of least-squares fits of the data by a proposed model (From Burnett et al., 1989).

& Payne, 1988), with sufficient laser power and excited-state lifetimes, all neutral species with excitations in resonance with the photon field and with appropriate ionization potentials are converted quantitatively into ions. Due to the pulsed nature of the experiment and the selective nature of the ionization process itself, the resulting ions may be efficiently counted by accelerating them with an external potential and measuring their TOF.

In this configuration the laser beam is focused in the shape of a ribbon 0.1 mm thick and 6 mm wide and directed 1 cm above and parallel to the target. Focusing allows ionization of those neutral species which are in a specific region of space. Hence, by varying the time difference between a 200-ns ion pulse and a 6-ns laser pulse, the velocity distribution of the neutral species is determined. Furthermore, the resulting ions may be imaged onto a microchannel plate which allows the position of the neutral species in the laser beam to be determined with

respect to the position of the incident ion beam on the target. With knowledge of the nature of the extraction fields and instrumental factors associated with TOF measurements and position-sensitive detectors, it is feasible to calculate the take-off angles of the neutral species (Kobrin et al., 1986). This apparatus was also suitably equipped with LEED for surface crystallography measurements and AES for surface cleanliness monitoring. This energy- and angle-resolved neutral (EARN) detector is a powerful device for measuring neutral trajectories with enormous sensitivity. Typically, a full EARN measurement can be recorded with a dose of 10^{12} Ar^+ ions/cm^2.

4 Experimental Studies of Single Crystal Bombardment

4.1 Yield Measurements

Although extensive effort has been devoted to measuring the total yield of particles emitted from polycrystalline targets bombarded at normal incidence, not many of these measurements have been reported on single crystals since the 1960's (Magnuson & Carlston, 1963). These workers used a weight loss technique to determine that the yield of Cu{100} is 2.0 times the yield of Cu{110} and 0.7 times the yield of Cu{111}. This trend, generally supported by computer simulations (Harrison et al., 1979), follows the trend of surface atom density in these materials. In general, these measurements are quite variable due to the ill-defined experimental conditions and are of only qualitative value.

An important recent measurement using nonresonant laser postionization powerfully illustrates the necessity of using clean well-defined surfaces under low dose conditions. As shown in Figure 3 the yield from Ru(0001) decreases by a factor of two as the dose is increased above $\sim 10^{14}$ ions/cm^2 for bombardment with 3 keV Ar^+ at normal incidence (Burnett et al., 1989). Since most other techniques require at least 1×10^{15} particles/cm^2, it is clear that those studies are tainted by significant surface damage effects. For the Ru case, it is tentatively proposed that the decrease in yield arises from the primary ion going into defect sites created by previous bombardment. As seen in the Figure, this model fits well with the experimental data, although there are a number of adjustable parameters in it. This idea needs to be further tested since it does not seem likely, based on the results of recent molecular dynamics computer simulations (Harrison, 1988). It would be valuable to see similar studies on other materials and at various temperatures.

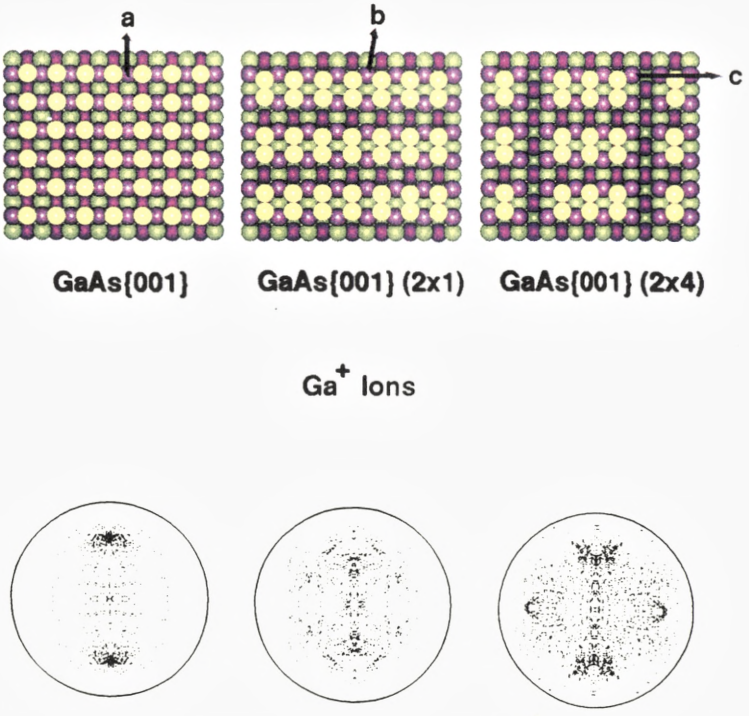

Figure 9. Top panel: Representations of three hypothetical GaAs{001} surfaces. The yellow balls represent surface As atoms. The purple balls represent second-layer Ga atoms and the green balls represent third layer As atoms. Bottom panel: calculated angular distributions of 10-30-eV Ga^+ ions desorbed by keV Ar^+-ion bombardment of the corresponding GaAs{001} surface given in the top panel. The <011> azimuthal crystal direction is parallel to arrow (c) in the figure. The polar angle of Ga^+-ion emission is proportional to the distance of a spot from the center of the circle. Ion ejection mechanisms (a), (b) and (c) are discussed in the text. (From Blumenthal et al., 1991).

requires the use of many-body potential functions. On the other hand, the lattices are much more transparent to the primary particle so that nuclear positions play a more dominant part in controlling the dynamics than the chemical bonding forces. The fact that the knowledge of the dynamics is not as extensive for semiconductors as it is for metals provides an added incentive for more effort in this area.

It is easy to examine the influence of the structure of the first atomic layer on the angular distribution of sputtered atoms from inspection of Figure 9. This figure shows on the left side a hypothetical unreconstructed GaAs{001} arsenic-terminated surface consisting of a square array of As atoms bonded to two Ga atoms

in the layer below. Each As atom possesses two partially filled 'dangling bonds' pointing upwards and oriented parallel to the <001> directions. The As atoms may pair up to form dimers along this direction, doubling the lattice periodicity, also shown in Figure 9. In the laboratory, the (2×1) reconstruction is not observed for GaAs but is for Si and C. Instead a series of structures is found, the most important of which is the As-rich (2×4) geometry shown in the right most panel. This structure is found during MBE growth of single-crystal GaAs films (Pashley et al., 1988; Biegelsen et al., 1990).

Molecular dynamics calculations are not yet available for GaAs. It is possible, however, to approximate the GaAs response to bombardment with a Si lattice since they both have related bonding properties and identical crystal structures. Results of molecular dynamics calculations for Si{001}, Si{001}-(2×1) and Si{000}-(2×4) are shown in the bottom part of Figure 9. The computational details have been discussed elsewhere (Smith et al., 1989). The distributions are displayed in a format which allows a real-space comparison to the model crystals of GaAs shown above them. The azimuthal angles are defined relative to the center of each circle. The polar angle is related to the distance of a spot from the center of the circle. These distributions are for the second-layer Si atoms which are found to eject. This set is crystallographically equivalent to the Ga atoms shown by the shaded atoms of Figure 1.

In a qualitative sense, the results of these calculations are quite fascinating. For the unreconstructed GaAs{001} surface, the Ga distribution exhibits only two peaks, at $\phi = 90°$ and 270°, with no structure found at higher polar angles and no intensity at $\phi = 0°$ and 180° or θ <45°. A detailed analysis of the atomic trajectories leading to these distributions suggests that the anisotropy arises from a direct mechanism whereby a third-layer As atom collides with a second-layer Ga atom and thereby causes the Ga atom to eject along their mutual bond axis (mechanism a). This mechanism can be ascribed to the directional bonding and open structure of covalent crystals and is rarely observed on metal surfaces. A graphical example of this mechanism is shown in Figure 10 at the top. The effect of the (2×1) and (2×4) reconstructions is also clearly visible through a broadening of the major spots (mechanism b) and by the appearance of intensity at $\phi = 0^0$ and $\phi = 180^0$, respectively. The mechanisms associated with these processes are somewhat varied, but have all been identified. A graphical example of mechanism c is shown in the bottom of Figure 10.

The experimental results for Ga^+ ions sputtered from GaAs{001}-(2×4) bombarded by 1 keV Ar^+ ions are shown in Figure 11. Although the laser postionization experiments have yet to be performed on this surface, related studies on GaAs{110} suggest that the ion and neutral distributions are quite similar (Blumenthal et al., 1990). Note that the general features predicted by the calculations are clearly

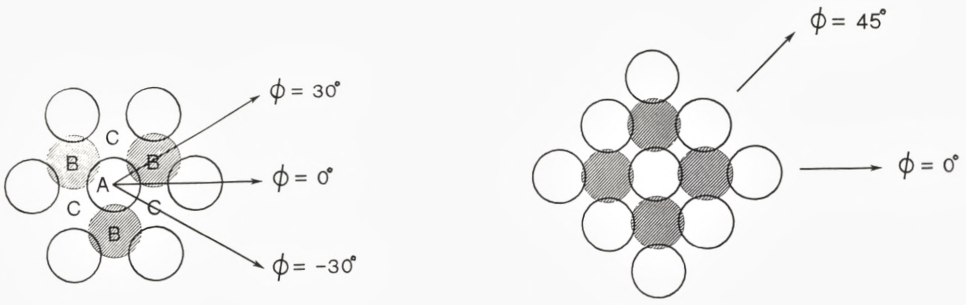

Figure 4. Schematic representation of our scheme for representing crystal directions for an fcc{111} and {001} face. A polar angle $\theta = 0°$ is normal to the surface. Open circles designate first- layer atoms and shaded circles second-layer atoms. The letters A-C designate possible adsorption sites for oxygen atoms.

4.2 Depth of Origin of Emitted Particles from Single Crystals

In order to have a proper mechanistic view of the sputtering event, it is of course essential to be certain about from where the emitted particles originate. Controversy about this subject dates to the original model by Sigmund (1969) where it was implied that particles could be emitted from below the surface layers. Later, computer simulations (Harrison et al., 1978) showed that for copper single crystals >90% of the particles are emitted from the top layer. A corrected sputter depth has recently been given (Vicanek et al., 1989) which is consistent with simulations.

Experimental tests of this idea on monoelemental targets are not available. Ideally, it would be interesting to create a single crystal target with an isotope whose surface layer is different from the bulk and study it using laser postionization detection. Several workers have attempted to come close to accomplishing this goal. Prigge and Bauer (1980) measured the W^+ yield from W{110} covered with varying amounts of Cu, Ag and Pd. Although the results are subject to many artifacts, their studies show that the W^+ signal disappears between one and two monolayers of deposited overlayers.

The most definitive experiment on well-defined single crystals was carried out on Ru{0001} covered with known amounts of Cu (Burnett et al., 1988) and bombarded at normal incidence by 3.6 keV Ar^+ ions. The experiment is particularly nice since they employed low dose, LEED/Auger and used MPRI postionization for detection. Moreover, Cu is known to form two-dimensional rafts on Ru, rather than multilayer structures. The results clearly show that virtually all of the emitted particles arise

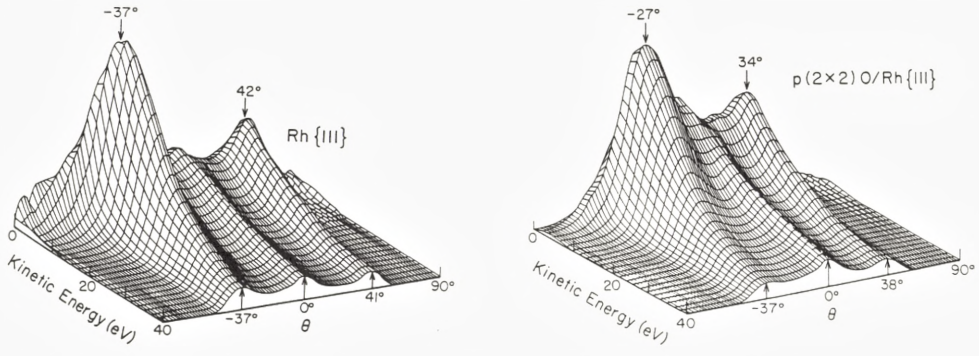

Figure 5. EARN intensity maps for clean Rh{111} and p(2×2) O Rh{111}. The plots are normalized to the highest intensity peak in both cases. The positive values of θ are recorded along $\phi = +30°$ and the negative values of θ are recorded along $\phi = -30°$ (From Winograd et al., 1986). Note that in the older spot notation, the [110] spot would occur at $\theta = 35.3°$ and $\phi = -30°$ and the [100] spot would occur at $\theta = 54.7°$ and $\phi = +30°$.

from the first layer.

Is this the final answer? No, there are a number of systems where the depth of origin is probably more than one layer. Computer modeling of Si{001}, for example, (Smith et al., 1989) clearly shows that particles can be emitted from the fourth or fifth layer. There is no direct experimental evidence for this prediction yet, but recent studies on GaAs{001} by Burnham et al. (1993) indicate that fourth layer Ga atoms can contribute significantly to observed angular distributions. Recent studies using the scanning tunneling microscope (STM) also suggest that deeper layers are exposed by single ion impacts on Si single crystals (Feil et al., 1992). If these results are correct, they may be important in understanding depth profiling in these commercially important materials.

4.3 Energy and Angular Distributions from Metallic Single Crystals

As was true during the time of Wehner's early experiments, accurate EARN distributions from well-defined surfaces are important for testing various theoretical models. Rhodium represents an important prototypical system for model studies. As seen in Figure 1, the electronic structure of Rh is well-suited for state-selected MPRI studies. Moreover, the surface chemistry of Rh has been extensively investigated by many techniques, and the surfaces are known to exhibit minimal surface relaxation or reconstruction that might complicate the analysis (Shepherd et al.,

1978).

Let us first consider the {111} face bombarded at normal incidence by 5 keV Ar^+ ions (Winograd et al., 1986). The crystallographic definitions for this face are defined in Figure 4, and the EARN data are shown in Figure 5. Note that for this crystal face, the surface atoms exhibit six-fold symmetry. The three second-layer atoms, however, create bulk three-fold symmetry with characteristic directions along <111> ($\phi = 0°$ in our notation), <211> $\phi = -30°$, and <112>, $\phi = +30°$. Experimental EARN results for $\phi \pm 30°$ are shown in Figure 5. Note that the results are qualitatively similar to many of the early data taken under much more trying circumstances. In Wehner's nomenclature, there would be a set of 3 weaker spots (ϕ = 30°, 150° and 270°), 3 stronger spots (ϕ = -30°, 90° and 210°), as well as a very weak central spot. The intensity along the closest- packed line of atoms in the surface plane ($\phi = 0°$, 60°, $\cdots$) is not shown but exhibits a minimum in intensity. The energy distributions are clearly dependent on the take-off angle, suggesting that their final energies are influenced by surface-layer collisions.

This directional nomenclature is different from that previously associated with single crystal sputtering. The reason for this change is that the older notation was based on the assumption that the anisotropy arose primarily from focused collision sequences deep within the crystal. Therefore, it was natural to define the 'spots' using bulk crystallographic directions. Now, we know that surface processes are the main contributors to the angular anisotropies. It is essential, therefore, that we adopt a notation that reflects this process and is consistent with the notation employed by the surface physics community.

With present-day computers, it is possible to utilize molecular dynamics computer simulations to try to reproduce the experimental results shown in Figure 5. These calculations are important to carry out for two reasons. First, they tell us whether a molecular dynamics model is sufficient to describe the formation of the collision cascade and the subsequent trajectories of ejecting atoms. Second, they allow us to examine the microscopic mechanisms that give rise to the angular anisotropies. The comparison between theory and experiment provides a modern-day reality check.

The details of the molecular dynamics scheme in general are described elsewhere in this book (Robinson, 1993; Nieminen, 1993). The details of the procedure for calculating EARN distributions for Rh have been described in detail and will not be discussed here (Garrison et al., 1988; Foiles et al., 1986). As seen in Figure 6, however, it is clear that for Rh{111}, at least, the comparison between calculation and experiment is about as good as can be expected over a wide range of phase space.

The calculations tell us that the collision sequences are strongly dominated by

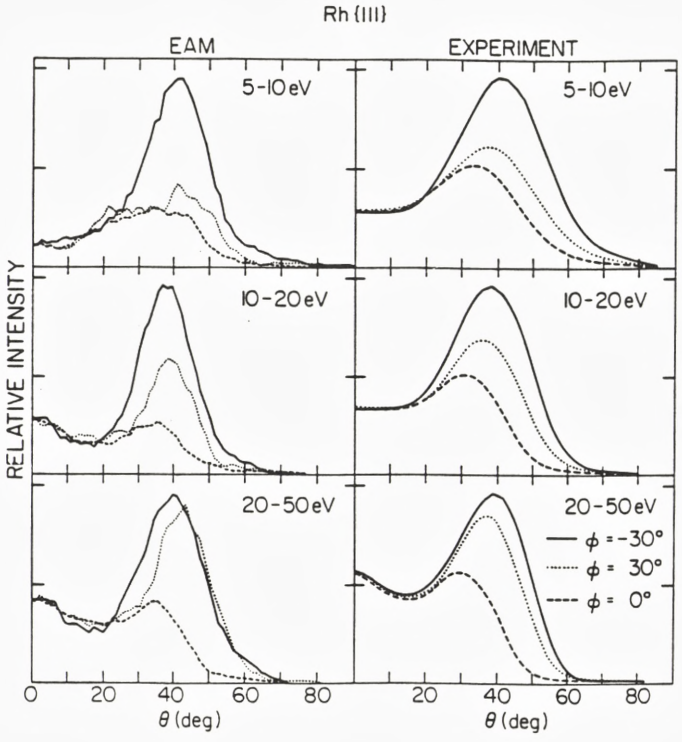

Figure 6. Polar angle distributions for various azimuthal angles for fixed secondary kinetic energy of the Rh atoms. In each frame the data are normalized to the ϕ = -30° peak intensity. The calculated data using the EAM potential are reported with a full width at half-maximum (fwhm) resolution of 15° in the polar angle. A constant solid angle is used in the histogramming procedure. The experimental resolution is also approximately 15°. The surface normal corresponds to $\theta = 0°$.

the alignment of atomic motions inside the solid. As these motions cause ejection of first-layer atoms, further focusing is caused by channeling or blocking by other first-layer atoms. Note that this type of channeling occurs at lower energies than that often associated with higher speed phenomena. For example, the highest intensity is observed along the open crystallographic directions ($\phi = \pm$ 30° in our case), and the minimum intensity is observed along the close-packed crystallographic direction (ϕ= 0°). If only the top surface layer was important, the peaks at θ = -37°, ϕ = -30° and θ = +42°, ϕ = +30° should be equal in intensity and not unequal as shown in Figure 5. The additional intensity at θ = -37°, ϕ = -30° arises mainly from the ejection of atom A by atom B (Figure 4) with first-layer focusing by other surface atoms. The peak at θ = +42° and ϕ = +30° is lower in intensity by a factor of

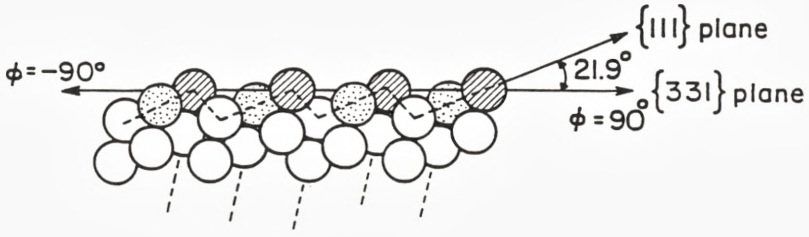

Figure 7. Cross-sectional view of the Rh{331} surface.

0.5 at low kinetic energy since no such mechanism is available along this azimuth. The peak at $\theta = 0°$ has a large component from ejection of the second-layer atom B which is focused upward by three surface atoms.

Many earlier experiments have been reported on {111} surfaces. Szymczak & Wittmaack (1980) found for 4 keV Ne^+ on gold, for example, that the peak along ϕ = -30° (the [011] spot in their notation) was at least 4 times the intensity of the peak along $\phi = +30°$ (the [100] spot). No intensity above a cosine background was observed at normal emission. The results are important since they show that the overall intensity directed into the spots is quite high, up to 50% in favorable cases. They are quantitatively different from the results found for Rh{111}, however, in that there is less of a difference found between ϕ = -30° and $\phi = +30°$ and there is a small amount of intensity found at normal emission for Rh{111}. It is unlikely that the distributions reported by Szymczak and Wittmaack could be reproduced by the computer modeling as these calculations would probably yield results very similar to those found on Rh{111}. Without further experiments and calculations, however, further hypothesizing about these differences would be mere speculation.

Another study of Ni{111} bombarded by 1.1 keV Ne^+ ions at normal incidence has recently been reported by Wucher et al. (1992). Their angular distributions, which are energy selected, are very similar to those found on Rh{111}. For example, they find that only the relatively high energy particles are emitted at normal incidence as shown in Figure 6. The major difference arises from the observation that the $\phi = +30°$ peak is several times more intense than the ϕ = -30° peak after the background is removed. Their computer modeling suggests these two features should be much closer in intensity as suggested by the data for Rh{111} shown in Figure 6. Since their experiments were not performed in the low-dose regime, it is difficult to speculate about the cause of this discrepancy.

How do these measurements and interpretations jive with earlier models of the production of angular anisotropies? This is a very tricky question. Mechanis-

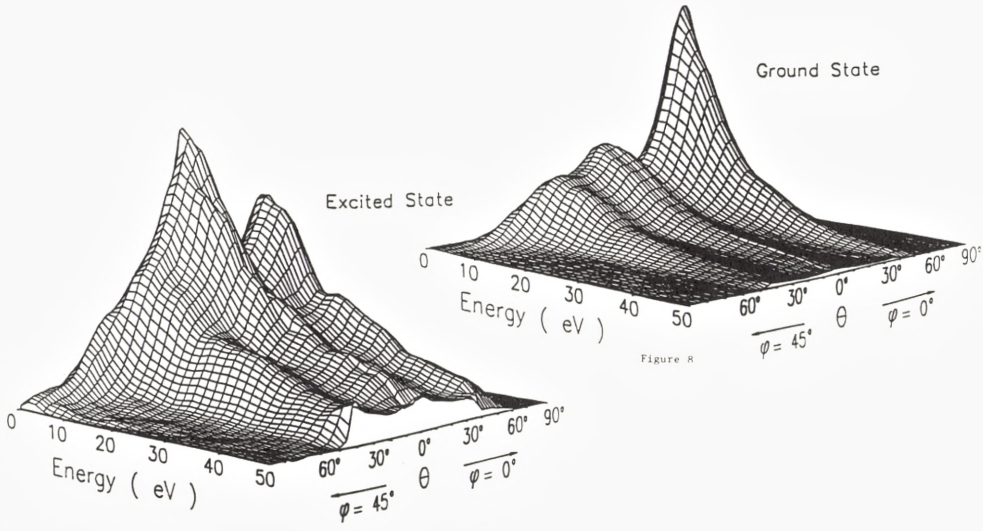

Figure 8

Figure 8. Energy- and angle-resolved distributions of Rh atoms in the $^4F_{7/2}$ excited state and $^4F_{9/2}$ ground state, ejected from 5 keV Ar^+ ion bombarded Rh{100}. The data correspond to ejection along $\varphi = 0°$ (<100>) and $\varphi = 45°$ (<110>) crystallographic directions, as defined in the inset. Due to the symmetry of the surface and the angular resolution (e.g., $\triangle\varphi = \pm 8°$ at $\theta = 45°$), the results represent the data over $\sim 50\%$ of all space. Both plots are normalized to the maximum intensity peaks. See Figure 4 for definitions.

tic conclusions drawn from molecular dynamics calculations involve an analysis of thousands of trajectories in an attempt to extract the essential physics. As Harrison has often illustrated (1988), the atom ejection process is associated with a cataclysmic event. Although explanations of the angular anisotropies for Rh{111} arise from such an analysis, there are many other mechanisms which also contribute significantly to sputtering. It is often not possible to distill all this particle motion into simple pictures. The critical issue here is that the molecular dynamics calculations can, for the first time, provide quantitative agreement with experiment, at least for Rh{111}. The important mechanisms are embedded in the computer printouts and are available for the taking even though with considerable difficulty. This degree of certainty has never been available before.

Given this caveat, there appears to be a great deal of similarity between the notions originally presented by Harrison et al. (1966), by Lehmann and Sigmund (1966) and by the most recent studies - as long as you do not look too closely. The early work focused attention on mechanisms involving transparency effects, lens effects and specific force fields. Both Lehmann and Sigmund mechanisms are quite reasonable in light of the molecular dynamics studies, although they begin to

break down when you ask questions about the energy dependence of the angular distributions. Their model would also predict that there should be no intensity in the $\phi = +30°$ direction. The key question, then, involves the generality of the mechanisms discussed above when applied to a variety of other systems.

If channeling and blocking in the first layer are important in controlling the angular distributions, there should be similar trends found on other crystal faces. Rh{331} is an interesting surface since it is a stepped structure with a (111) terrace that is three atoms wide. It is very similar to the {111} face except that it is tilted by 21.9° as shown schematically in Figure 7. The experimental results show that the ejection is strongly peaked along the $\phi = +90°$ azimuth, and that desorption along other crystallographic directions is considerably reduced (Reimann et al., 1989). Molecular dynamics calculations show that the $\theta = 15°$ peak arises from the same surface channeling mechanism operative for {111} corresponding to the $\theta = 37°$ peak along $\phi = 0°$. The reduced intensity along the other directions arises either from the presence of open channels in the crystal (near $\theta = 0°$) or from blocking due to the atomic step along ϕ = -90°.

Similar anisotropies are observed for Rh atoms desorbed from ion-bombarded Rh{001} (Maboudian et al., 1990; El-Maazawi et al., 1991). The experimental EARN distribution for this surface is shown in Figure 8. The highest intensity is found along the open crystallographic direction, $\phi = 0°$, while a minimum intensity is observed along $\phi = 45°$. A comparison between the polar angle distributions for Rh{111} and Rh{001} reveals additional details about the surface channeling and blocking mechanisms. It turns out that the peak in the polar angle distribution in the 10-20 eV range is larger for {001} ($\theta_{max} = 40°$, $\phi = 0°$) than for {111} ($\theta_{max} = 37°$, ϕ = -30°). This difference arises since the open channel is larger on {001}, allowing more grazing take-off angles. The polar angle intensity maxima along the close-packed directions, however, are nearly identical for both crystal surfaces ($\theta_{max} = 34°$ for {001} and $\theta_{max} = 32°$ for {111}). This result is important since the distance to the nearest-neighbor atom along the close-packed direction is identical for both surfaces. Thus, the polar angle distributions are determined by the extremely local interactions experienced by the desorbing atom, and can be predicted from the presence or absence of surface channeling directions.

Since crystal structure via surface channeling and blocking strongly influences the EARN distributions, it follows that adsorbate atoms or molecules on single-crystal substrates should systematically alter the trajectories of the desorbing underlayer species. The concept has been tested in detail for the p(2×2) O ordered overlayer on Rh{111} with the EARN experiment (Winograd et al., 1986; Reimann et al., 1989). For an atomic adsorbate of this sort, there are a number of possible high-symmetry binding sites including two different 3-fold hollow sites (often referred to as the **B** or hcp site and the **C** or fcc site) and an on-top site (or **A** site)

as shown in Figure 4. The simplest idea is that adsorption of oxygen atoms at a **B** site should preferentially block Rh atoms desorbing along the $\phi = +30°$ azimuth, adsorption at a **C** site should alter Rh atoms leaving along $\phi = -30^0$ while **A** site adsorption may have very little effect, except perhaps on the particles emitted at $\theta = 0°$. Polar angle measurements as seen in the lower part of Figure 4 clearly show that the $\phi = -30°$ direction is preferentially reduced relative to either $\theta = 0°$ or $\phi = +30°$ strongly suggesting **C** site adsorption.

These results are quite interesting since they clearly show how sensitive the desorption angular distributions are to small overlayer coverages. In this case, in addition to the observed perturbations in the EARN distributions, the total ground state neutral Rh atom yield was observed to decrease by a factor of about 2 (Reimann et al., 1989). These observations further illustrate that trajectory measurements which are to be compared with theory must be performed on well-cleaned and characterized surfaces and under low-dose conditions.

4.4 Energy and Angular Distributions from Semiconductor Single Crystals

Angular anisotropies have also been observed for atoms ejected from ion-bombarded single crystal semiconductor surfaces. The earliest observations (Southern et al., 1963) indicated that the anisotropies were smaller than for metals. Later, however, it was discovered that the angular distributions were strongly temperature dependent, suggesting that crystal damage and thermal annealing were complicating the analysis (Anderson et al., 1963). Because of the technological importance of Si, GaAs and related materials, many studies of the topological changes that occur due to extensive bombardment have been reported (Carter et al., 1984). Only recently have well-defined surfaces prepared under UHV conditions been studied in detail. What emerges is a fascinating comparison between the dynamics of sputtering in metals with that found in the more open covalent lattice of semiconductors.

GaAs{001} represents an extraordinary model semiconductor surface. Depending upon how it is grown, the surface can be terminated with various coverages of As or Ga (Arthur, 1974; Neave & Joyce, 1978). It crystallizes with a zinc blende lattice, the same as Si, which means that the 001 plane exhibits alternating layers of As and Ga atoms. Moreover, the surfaces exhibit a well-defined rearrangement that has been characterized by scanning tunneling microscopy (Pashley et al., 1988) and by various diffraction techniques. The surfaces are normally prepared using molecular beam epitaxial growth (MBE) methodology (Arthur, 1974).

Molecular dynamics computer simulations have only recently been attempted for semiconducting materials (Stansfield et al., 1989; Smith et al., 1989). The calculations are more difficult in the sense that there is directional bonding which

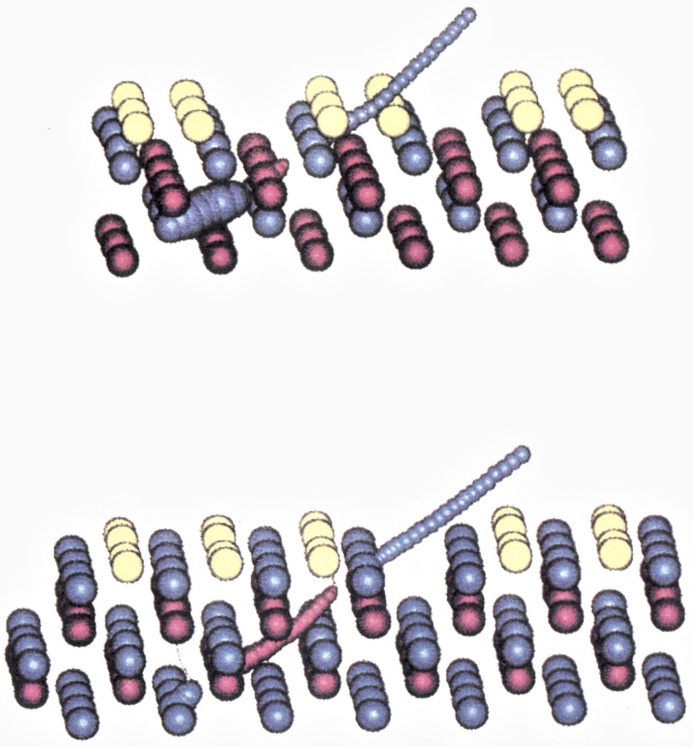

Figure 10. Top: The direct ejection mechanism which is responsible for the two dominant features in the GaAs{001}-(2×4) secondary ion distribution. The mechanism is characterized by a direct momentum transfer between a third layer As atom and a second layer Ga atom along their bond axis in the <110> direction. The Ga atom may eject over the channel between As_2 dimers or up through the As_2 dimers as pictured. Bottom: The desorption of a second layer Ga atom in the <110> direction across the missing dimer row. The pictured collision sequence shows a lower layer As atom channeling up through the crystal and transferring momentum to the Ga atom. The Ga atom may desorb at a high polar angle since it ejects across the missing dimer row. The momentum transfer in this direction is not as efficient as in the <110> direction which causes the desorbed ion intensity to be lower.

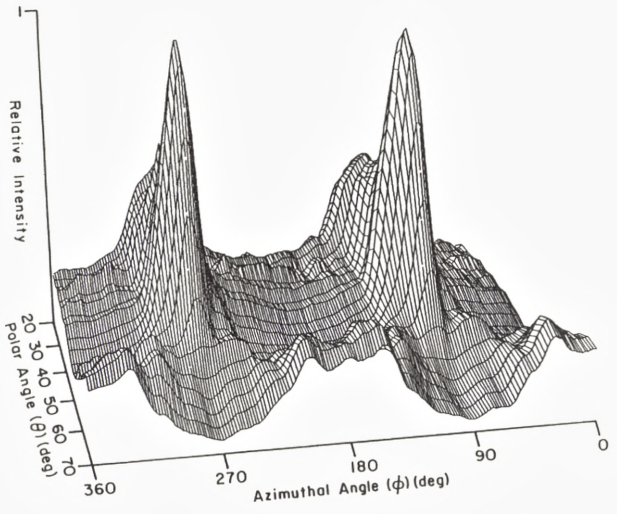

Figure 11. The relative intensity of 20-eV Ga^+ ions desorbed by 3-keV normal incident Ar^+-ion bombardment of the GaAs{001}-(2×4) surface. The polar angle is the angle of detection from the surface normal. For the in-plane azimuthal angle, $\phi = 0°$ corresponds to the <011> crystal direction.

visible and that the influence of the reconstruction can be seen at higher polar angles as expected (Blumenthal et al., 1991). These experiments are continuing with a special emphasis on how the features should change during deposition of thin metallic overlayers such as Al. It would also be interesting to be able to measure the As emission, although at the present time it is experimentally intractable.

5 Angle of Incidence Effects - Shadow-Cone Enhanced Desorption

Much of what we have learned about angular distributions so far is derived from experiments carried out at normal incidence, partly because the dynamics calculations are easier under these conditions, and partly because of experimental convenience. It is well-known from the early literature, however, that the angle of incidence of the primary particle significantly influences the sputtering yield. Early experiments on single crystals, for example, suggested that the yield of particles is reduced when the angle of incidence occurs along a channeling direction and that it is increased when the particle is incident upon a random direction (Magnuson & Carlston, 1963; Robinson & Southern, 1967).

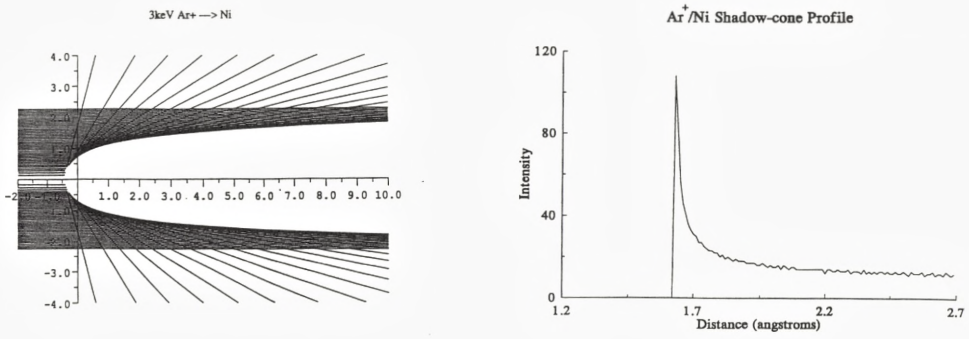

Figure 12. Left: The trajectories from the interaction of a 3 keV Ar^+ ion beam with a Ni atom. The incident ions are deflected and a region of zero ion flux is created behind the Ni atom. The edge of this region defines the shadow-cone. All distances are in Ångströms. Right: A profile of the shadow-cone 5 Å behind the Ni atom which illustrates the focusing effect.

There is another issue relevant to this discussion which is embedded in the dynamics of the atomic motion. That is, specific impact points on the surface exhibit very high yields while other points are rather inactive for sputtering. This observation led to the concept of atoms sputtered per incident ion or ASI distributions (Harrison, 1988). For 1 keV Ar^+ ion on Cu, for example, the Cu yield varies from 0 to over 15, depending on the impact point. It would be interesting to be able to find these high action points in the laboratory, a dim prospect considering the aiming accuracy required.

It is possible to take advantage of the above information to utilize the angle of incidence of the ion beam to glean even more detailed information about surface structure. The collision of the primary ion with a surface atom creates a shadow-cone which focuses the incident flux to specific surface coordinates (Van der Veen, 1985). Shadow-cones have been discussed extensively since their discovery by Lindhard (1965). As seen in Figure 12 for 1 keV Ar^+ on a Ni atom, this flux is sharply peaked at the shadow-cone edge and exhibits a width of less than 0.02 Å. When the tail of this shadow-cone strikes a surface or near-surface atom, the desorption yield should dramatically increase. In effect, we can 'aim' the incident beam to specific high action points in the target. With knowledge of the shadow-cone shape, it is then feasible to determine surface geometries using simple triangulation. The strategy is reminiscent of impact collision ion scattering spectrometry (ICISS) where it is possible to detect the crystal orientation which gives rise to incident ions that are backscattered by 180° (Aono et al., 1981; Aono et al., 1983; Yarmoff et al., 1986).

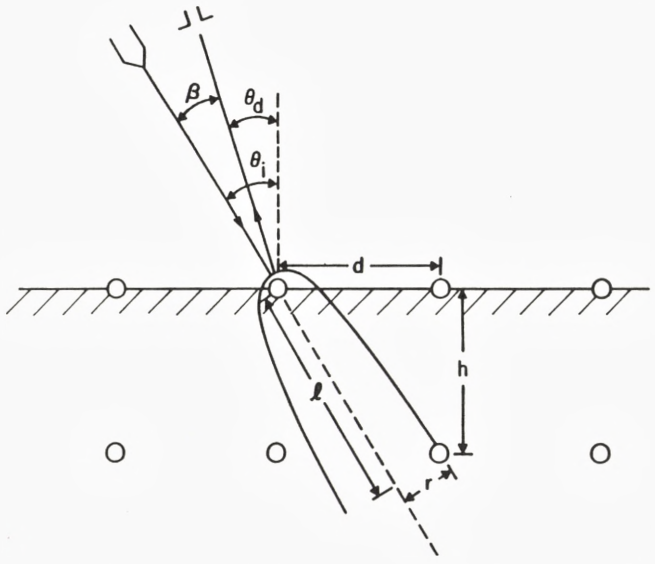

Figure 13. Parameter definitions for the shadow-cone-enhanced desorption experiment. The ion beam is incident at θ_i, the desorbed particles are detected at θ_d and $\beta = \theta_i - \theta_d$. The shadow-cone is described by a radius **r** at a distance **l** behind the target atom. The **d** and **h** values describe the surface bond lengths.

The geometry of the shadow-cone enhanced desorption experiment is illustrated in Figure 13. In principle, the detector should be configured to collect all desorbing ions, regardless of their kinetic energy or angle. Most experiments to date, however, have been performed with a fixed angle β and with a detector set to collect only the high-kinetic-energy particles. With this configuration, the shadow-cone enhanced desorption concepts may be more carefully evaluated (Chang et al., 1987). Moreover, it has been shown (Chang & Winograd, 1989) that for θ_d between $\pm 45°$, ion neutralization effects are not of sufficient magnitude to shift the angles of the intensity maxima, although the relative position of the peaks may be altered somewhat. This is a convenient geometry, then, for indirectly examining the behavior of neutral atom ejection.

Representative results (Chang & Winograd, 1989) for Ag{110} are shown in Figure 14. There are two major features in these distributions which correspond to intersection of the shadow-cone with a second-layer atom ($\theta \sim 35°$) and with a first-layer atom ($\theta \sim 70°$). The fact that these peak maxima actually correspond to the intersection of a shadow-cone edge with a substrate atom has been tested by using a full three-dimensional computer simulation. The position of this peak has

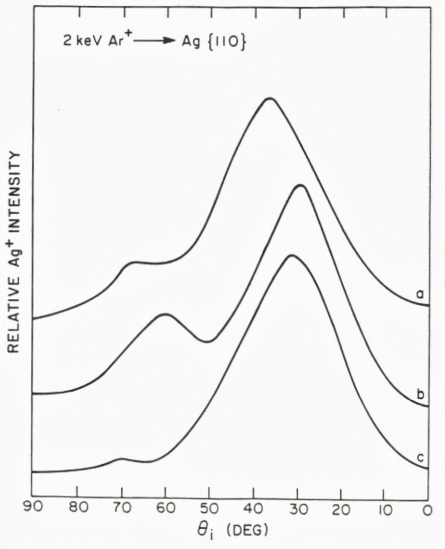

Figure 14. The shadow-cone enhanced SIMS spectra of the desorbed Ag^+-ion yield as a function of the angle of incidence. The particles are collected along the (a) <100>, (b) <110> and (c) <211> azimuth during 2-keV Ar^+-ion bombardment at a current of ~5 nA. Only particles desorbed in plane with $\beta = 25°$ are collected. (From Chang & Winograd, 1989).

been shown to be unaffected by the image interaction or other forces related to the secondary ionization process since the peak position is found to be independent of β for θ_d values between 0° and 45°. From the position of the peaks, it is possible to calculate **d** using a Moliere potential and to compare this calculated value to the known interatomic spacing for Ag. The results compare to within ± 0.5°, yielding an uncertainty of about ±0.06 Å in the bond length. Similar procedures for determining **h** suggest that the spacing between the first and second layer is relaxed by (7.8 ± 2.5)% and the spacing between the first and third layer is relaxed by (4.1 ± 2.1)% relative to the bulk spacing. These values agree within the same error limits with those bond lengths found by Rutherford backscattering measurements (Kuk & Feldman, 1984).

Adsorbate atoms will also create shadow cones that can intersect nearby substrate atoms, opening the possibility of measuring the bond length of chemisorbed species. An excellent case to test this idea is the chemisorption of Cl on Ag{110}. Channeling and blocking experiments suggest that the Cl atom binding site is invariant over a wide coverage range, allowing the Ag-Cl bond length to be examined under a variety of experimental conditions (Chang et al., 1987; Winograd & Chang,

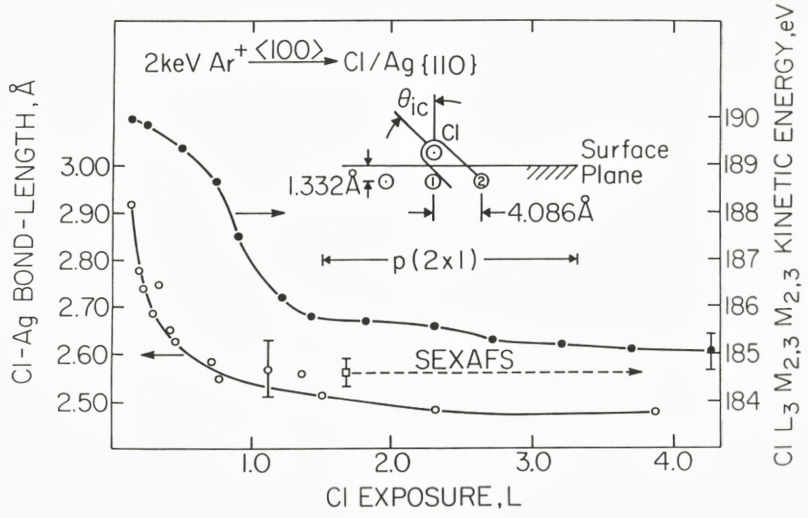

Figure 15. Ag-Cl bond-length change (○) and Auger Cl $L_3M_{2,3}M_{2,3}$ kinetic energy (●) as a function of Cl_2 exposure at 300 K. The reported value refers to the distance between the center of silver atom 1 and the Cl atom. The p(2×1) LEED pattern was observed in the exposure region as shown. The bond lengths from the SEXAFS experiments are associated with the LEED pattern; the same value was also obtained at a coverage beyond 4 L and associated with the c(4×2) LEED pattern. The shadow-cone induced desorption mechanism used to calculate the bond length is shown in the inset. The interplanar spacing refers to the relaxed clean-surface Ag{110} value. The shadow-cone shape was calculated using a Thomas-Fermi-Moliere potential with a scaling factor of 0.86. (From Winograd & Chang, 1989).

1989). The results for the shadow-cone experiments are shown in Figure 15. Of particular note is that at extremely low Cl coverages, the observed bond length is extended over that observed in the high coverage limit by nearly 0.4 Å. This change in length, accompanied by a change in the shape of the Auger electron emission spectra, has been explained as being due to a shift from highly ionic bonding at low coverage to more covalent bonding at high coverage. If the Ag-Cl interaction is highly ionic, the bond should have a significant dipole moment. Presumably dipole-dipole interactions between nearby Cl^- atoms force charge back into the Ag substrate. The absolute value of the bond length at high exposures agrees quite well with surface-EXAFS experiments obtained from the p(2×1) ordered overlayer (Holmes et al., 1987) as seen in Figure 15. The results are also consistent with the channeling and blocking experiments discussed previously, which suggest that the Cl adsorbate could more closely approach the surface at higher coverages (Moon

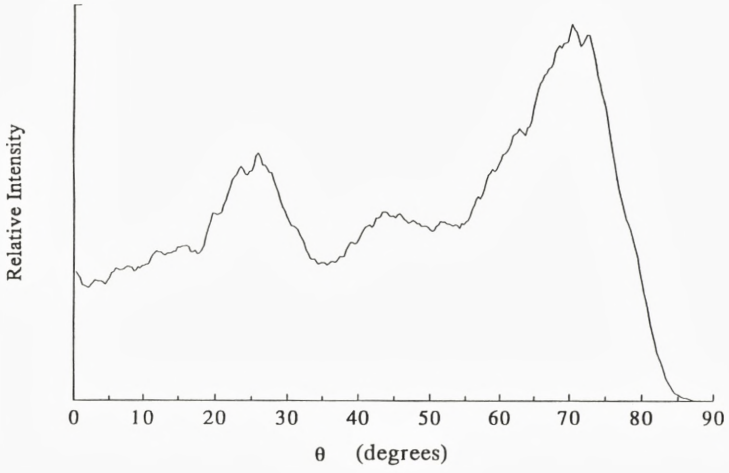

Figure 16. The relative intensity of 20-eV Ga^+ ions desorbed from the GaAs{001}(2×4) surface by 3-keV Ar^+-ion bombardment, plotted as a function of the ion-beam polar angle, relative to the surface normal. The ion beam is parallel to the <011> crystal direction. (From Xu et al., 1992).

et al., 1986).

These types of surface structure determinations are readily extended to more complex systems. Of special interest are compound semiconductor surfaces, not only because of their technological relevance, but also because they display a rich diversity of surface structures which need to be characterized. A good example is GaAs{001}-(2×4) which was examined earlier in this review with regard to its behavior under bombardment at normal incidence. The most straightforward objective of the shadow-cone experiments would be to determine the length of the As-As bond in the surface layer. This number is difficult to obtain by other methods, but is important for input into calculations aimed toward predicting the surface electronic structure (Chadi, 1987; Larsen & Chadi, 1988).

The results of this experiment (Xu et al., 1992) are shown in Figure 16. The crystal direction, <011>, corresponds to shooting the incident beam directly along the As_2 bond, in an azimuthal direction parallel to the missing row of As atoms. The spectrum consists of four major peaks at polar angles of $\theta_i = 70.1°$, 63.0°, 44.5° and 25.8°. There are many other distinguishable features in the spectrum which have been confirmed to be real structure, but their interpretation awaits future generations of research students (Burnham et al., private communication). The main peaks have been assigned on the basis of parallel molecular dynamics

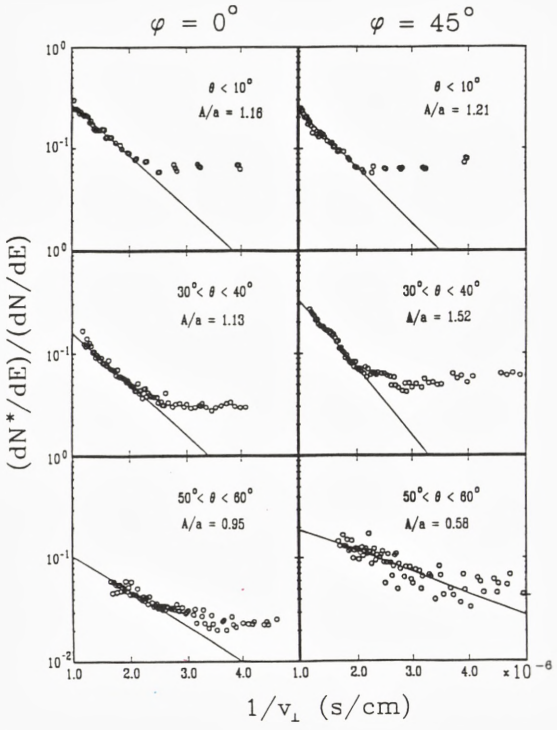

Figure 17. Ratio of intensities $(dN^*/dv/(dN/dv)$ vs $1/v_\perp$ for different angles of ejection. These data are direct ratios of the intensities given in Figure 1. The straight lines have been fit to the high velocity portion of the data and have a slope of A/a (in units of 10^6 cm/s) as displayed in each frame (From Shapiro & Fine, 1989).

calculations for Si (Xu et al., 1992). A summary of those results is given in Table I. Notice that the As_2 distance is determined from the small shoulder at 63° to be 2.73± 0.10 Å. The procedure for calculating the bond-length is identical to that described for the Ag{110} surface. This value of 2.73 ± 0.10 Å is within experimental error of a grazing-incidence x-ray diffraction value from GaAs{001} c(4×4) of 2.59 ±Å (Sauvage-Simkin et al., 1989). These numbers suggest that the dimer bond distance is much closer to the bulk As bond distance with threefold coordination than to a tetrahedral covalent As bond involving sp^3 hybridization (Kittel, 1986).

The fact that these simple angular distributions provide such microscopic information about surface structure is really remarkable from several points of view. Certainly, the primary beam is creating lots of damage to the surface, and yet it

Table I. Experimental and calculated results. Distances are expressed in Ångströms and angles in degrees. D_{11} is the first-layer As-As bond distance in a <011> direction; D_{22} the second-layer Ga-Ga distance along a <011> direction.

Crystal Direction	Peak	θ_i	D_{bulk}	D_{anal}	D
<011>	Peak 1	70.1	4.00	4.00 ± 0.10	D_{22}
	Peak 2	63.0	4.00	2.73 ± 0.10	D_{11}
	Peak 3	25.8	1.41	1.40 ± 0.10	D_{23}

seems possible to obtain accurate surface bond lengths. The experimental configuration is exceedingly straightforward, requiring only a simple ion source, quadrupole mass filter and polar angle rotation capabilities for the sample holder. The potential sensitivity of this approach to low concentrations of overlayers is indeed unprecedented. The three examples presented in this review are very promising ones, but much research remains to be accomplished in this area. It will be interesting to examine how the distributions change with shadow-cone radius and whether it will be possible to enhance certain desorption mechanisms by changing particle mass and energy. Perhaps the most important aspect of this experimental configuration, however, is that it allows an accurate description of the sputtering event to be performed without using molecular dynamics calculations. The angular distributions can be largely explained using only the details of the first encounter of the primary ion with the crystal surface.

6 Spectroscopic Studies of Single Crystal Sputtering

The laser techniques described in section III and IV are inherently state selective as illustrated in Figure 1. For example, the $^4F_{9/2}$ ground state can be ionized through the $^2F_{7/2}$ state with two 312.4 nm photons. The metastable $^4F_{7/2}$ state lies 0.2 eV above the ground state and can be ionized using two 328.0-nm photons. Since $^4F_{9/2} \leftarrow {}^4F_{7/2}$ is a forbidden transition, it is possible to make detailed measurements on both states and to compare the results directly. The comparison provides an unprecedented level of detail regarding the mechanistic aspects of energy excitation and quenching at surfaces.

A direct measurement of the complete EARN distribution for both the $^4F_{9/2}$ ground state and the $^4F_{7/2}$ excited state for Rh{100} has recently been completed (Winograd et al., 1992; Bernardo et al., 1992), and both maps are shown in Figure

8. Note that the intensity of the desorbed atoms in their ground state is very weak along the close-packed direction ($\phi = 45°$ as defined in Figure 3) due to blocking, as expected from the classical calculations. The open direction ($\phi = 0°$) largely arises from second-layer atoms being focused upward by first-layer atoms. The EARN map of the $^4F_{7/2}$ level is significantly different from the ground-state distribution. There is considerably more relative intensity observed at normal ejection ($\theta = 0°$). At low energies, only a shoulder exists along the $\phi = 45°$ azimuth (<110> direction). And finally, the falloff with energy is much slower for the excited state.

It is most likely that the population of the $^4F_{7/2}$ state is a direct measure of the excitation probability, uncomplicated by so-called cascading effects. This conclusion is derived from two important facts. First, the intensity of the ground-state signal is approximately 20 times the signal observed for the $^4F_{7/2}$ state. Second, the intensity of the next higher-lying excited state ($^4F_{5/2}$ with excitation energy of $\sim$ 0.3 eV above the ground state) is at least 2 orders of magnitude smaller than the $^4F_{7/2}$ state. Earlier studies by Young and co-workers (1984) using laser-induced fluorescence have shown that the population density for Fe decreases exponentially with the magnitude of the excited energy, roughly in accord with the observations for Rh. Similar results have been obtained using MPRI (Kimock et al., 1984). Hence, there are an insignificant number of excited Rh atoms in sufficiently high-lying excited states to contribute to the $^4F_{7/2}$ level by cascading from higher levels. Once these atoms reach the gas phase, then, it is unlikely that the population density is affected by decay from other excited states.

The interpretation of these energy and angle-resolved excitation probabilities are only now being sorted out. The general idea is to try to describe the dynamics of the excitation and deexcitation physics using known quantum mechanical phenomenon and then to examine the effects of this dynamics when it is coupled together with classical molecular dynamics (Bernardo et al., 1992). Several important concepts are emerging from these models. First, the form of the velocity dependence is strongly reminiscent of Hagstrum's (1954) original energy transfer ideas. A model which is consistent with this picture is currently being exploited by several groups and involves collisional excitation followed by nonradiative deexcitation (Bernardo et al., 1992; Shapiro & Fine, 1989). Both the excitation and deexcitation steps obviously depend upon the nature of the collision cascade as it evolves in the crystal and on the electronic properties of the material. For the data shown in Figure 17, note that the slopes of the change in the logarithm of the excited state fraction with $1/v_\perp$ depends on both polar and azimuthal angle. This effect is not predicted without including the influence of the cascade on the entire process (Winograd et al., 1992; Bernardo et al., 1992; Winograd, 1992). For example, if glancing collisions are important at high polar angles, the quenching rate will be appropriately higher.

Although there are many potential intricacies associated with these experiments, it is of interest here to conclude with one final observation. There is a region of the data shown in Figure 17 where the excited fraction is found to be independent of velocity. Although a number of factors contribute to this effect, the molecular dynamics calculations show that collisions of atoms over the surface are most important (Winograd et al., 1992; Bernardo et al., 1992; Winograd, 1992). With this mechanism, two independently ejected atoms undergo a hard collision over the surface and become reexcited. Because they are out of the electronic coupling range of the solid, the excitations are not quenched.

7 Conclusion and Prospects

The revolution in modern surface science has opened new opportunities for learning more details about single crystal sputtering than ever before. Moreover, new detection schemes have made it possible to essentially examine the collision dynamics on an event by event basis. The new data are now in quantitative agreement with results from sophisticated molecular dynamics calculations, at least for a limited number of model systems. This agreement allows one to extract the important energy dissipation mechanisms from the computer printouts and to have confidence in their validity.

Yet, there is much to be done. The computer simulations are complex and the experimentalists need simpler formulas by which to interpret their data. These formulae, however, should provide a quantitative prediction of the sputtering yield as a function of ejection energy and angle. Perhaps the shadow-cone approach, where the mathematics is easy, is a step in that direction. Spectroscopic studies of single crystal sputtering are only beginning and offer hope of disentangling the factors that go into inelastic energy loss. For example, the studies discussed here involved only electronic states that are part of the ground state manifold. Higher lying states will undoubtedly yield new surprises. And finally, there needs to be more work on molecular crystals, alloys or on insulating crystals in order to continue to elucidate the mechanistic differences associated with the sputtering of these disparate materials. Spectroscopic studies of neutral clusters emitted from single-crystals under low-dose conditions would provide interesting information about the vibrational and rotational excitations that occur in these species. There will certainly be many interesting new effects discovered with these substances. Their role is already becoming increasingly important in modern materials science.

Acknowledgements

The author greatly appreciates the critical reading of this manuscript by Barbara J. Garrison. He is also most grateful for the financial support of The National Science Foundation, The Office of Naval Research and The Department of Energy.

References

Anderson GS and Wehner GK, 1960: J. Appl. Phys. **31**, 2305
Anderson GS, Wehner GK and Olin HJ, 1963: J. Appl. Phys. **34**, 3492
Aono M, Oshima C, Zaima S, Otani S and Ishizawa Y, 1981: Jpn. J. Appl. Phys. **20**, L829
Aono M, Hou Y, Souda R, Oshima C., Otani S and Ishizawa Y, 1983: Phys. Rev. Lett. **50**,1293
Arthur JR, 1974: Surf. Sci. **43**, 449
Becker CH and Gillen KT, 1984: Anal. Chem. **56**, 1671
Bernardo DN and Garrison BJ, 1992: J. Chem. Phys. **97**, 6910
Bernardo DN, El-Maazawi M, Maboudian R, Postawa Z, Winograd N and Garrison BJ, 1992: J. Chem. Phys. **97**, 3846
Biegelsen DK, Bringams RD, Northrup JE and Swartz LE, 1990: Phys. Rev. **B41**, 5201
Blumenthal R and Winograd N, 1991: Phys. Rev. B15 **42**, 11027
Blumenthal R, Caffey KP, Furman E, Garrison BJ and Winograd N, 1991: Phys. Rev. B. **44**, 12830
Burnett JW, Biersack JP, Gruen DM, Jørgensen B, Krauss AR, Pellin MJ, Schweitzer EL and Yates Jr YT, 1988: J. Vac. Sci. Tech. **A6**, 2064
Burnett JW, Pellin MJ, Calaway WF, Gruen DM and Yates Jr JT, 1989: Phys. Rev. Lett. **63**, 562
Burnham JS, Goss SH and Xu C, 1993: private communication
Carter G, Navinsek B and Whitton JL, 1984: *Sputtering by Particle Bombardment II*, Ed., R. Behrisch, Springer-Verlag, Berlin, p. 231
Chadi DJ, 1987: J. Vac. Sci. Technol. **A5**, 834
Chang CC and Winograd N, 1989: Phys. Rev. B. **39**, 3467
Chang CC, Malafsky GP and Winograd N, 1987: J. Vac. Sci. Tech. A. **5**, 981
El-Maazawi M, Maboudian R, Postawa Z and Winograd N, 1991: Phys. Rev. B15 **43(14)**, 12078
Feil H, Zandvliet HJW, Tsai MH, Dow JD and Tsong IST, 1992: Phys. Rev. Lett. **69**, 3076
Foiles SM, Baskes MI and Daw MS, 1986: Phys. Rev. B **33**, 7983
Garrison BJ, Winograd N, Deaven DM, Reimann CT, Lo DY, Tombrello TA, Harrison Jr DE and Shapiro MH, 1988: Phys. Rev. **B37**, 7197
Gibson JB, Goland AN, Milgram M and Vineyard GH, 1960: Phys. Rev. **120**, 1229
Hagstrum HD, 1954: Phys. Rev. **96**, 6800
Hammer D, Benes E, Blum P and Husinsky W, 1976: Rev. Sci. Instrum. **47**, 1178
Harrison Jr DE, 1988: CRC Rev. in Sol. St. and Mat. Sci. **14**, S1
Harrison Jr DE, Johnson JP and Levy NS, 1966: Appl. Phys. Lett. **8**, 33
Harrison Jr DE, Levy NS, Johnson JP and Efron HM, 1968: J. Appl. Phys. **39**, 3742
Harrison Jr DE, Kelly PW, Garrison BJ and Winograd N, 1978: Surf. Sci. **76**, 311
Hauffe W, 1991: *Sputtering by Particle Bombardment III*, eds. R. Behrisch and K. Wittmaack, Topics in Applied Physics **64**, Springer-Verlag, Berlin, p. 305
Hofer WO, 1973: Rad. Effects **19**, 263
Hofer WO, 1991: *Sputtering by Particle Bombardment III*, Topics in Applied Physics **64**, Springer-Verlag, Berlin, p. 15

Holmes DJ, Panagiotides N, Barnes CJ, Dus R, Norman D, Lamble GM, Della Valle F and King DA, 1987: J. Vac. Sci. Technol. A **5(4)**, 703
Hurst GS and Payne MG, 1988: *Principles and Applications of Resonance Ionization Spectroscopy*, Adam Hilger, Philadelphia, PA
Hurst GS, Payne MG, Kramer SD and Young JP, 1979: Rev. Mod. Phys. **51**, 767
Jenkins LH and Chung MF, 1971: Surf. Sci. **29**, 125
Kimock FM, Baxter JP, Pappas DL, Kobrin PH and Winograd N, 1984: Anal. Chem. **56**, 2782
Kittel C, 1986: *Introduction to Solid State Physics*, 6th Ed., Wiley, New York, 76
Kobrin PH, Schick GA, Baxter JP and Winograd N, 1986: Rev. Sci. Instrum. **57**, 1354
Kuk Y and Feldman LC, 1984: Phys. Rev. **B30**, 5811
Larsen PK and Chadi DJ, 1988: Phys. Rev. **B37**, 8282
Lehmann C and Sigmund P, 1966: Phys. Stat. Solidi **16**, 507
Lindhard J, 1965: Dan. Vid. Sel. Mat. Fys. Medd. **34**, No. 14
Lundquist TR, 1978: J. Vac. Sci. Tech. **15**, 684
Maboudian R, Postawa Z, El-Maazawi M, Garrison BJ and Winograd N, 1990: Phys. Rev. B15 **42(12)**, 7311
Magnuson GD and Carlston CE, 1963: J. Appl. Phys. **34**, 3267
Moon DW, Bleiler RJ and Winograd N, 1986: J. Chem. Phys. **85**, 1097
Moore CE, 1971: *Atomic Energy Levels, U.S. Department of Commerce Report* NSRDS-NBS 35, Washington, DC
Neave JH and Joyce BA, 1978: J. Cryst. Growth, **44**, 387
Nelson RS, 1963: Phil. Mag. **8**, 693
Nieminen RM, 1993: Mat. Fys. Medd. Dan. Vid. Selsk. **43**, 81
Oechsner H and Gerhard W, 1972: Phys. Lett.**40A**, 211
Pashley MD, Habereen KW, Friday W, Woodall JM and Kirchner PD, 1988: Phys. Rev. Lett. **60**, 2176
Prigge S and Bauer E, 1980: In Advances in Mass Spectrometry, Vol. 8A, ed. Quale, A, Heyden, London, p. 543
Reid I, Farmery BW and Thompson MW, 1976: Nucl. Instrum. Methods **132**, 317
Reimann CT, El-Maazawi M, Walzl K, Garrison BJ and Winograd N, 1989: J. Chem. Phys. **90(3)**, 2027
Robinson MT, 1993: Mat. Fys. Medd. Dan. Vid. Selsk. **43**, 27
Robinson MT and Southern AL, 1967: J. Appl. Phys. **38**, 2969
Sauvage-Simkin M, Pinchaux R, Massies J, Calverie P, Jedrecy N, Bonnet and Robinson IK, 1989: Phys. Rev. Lett. **62**, 563
Schuhle U, Pallix JB and Becker CH, 1988: J. Am. Chem. Soc. **110**, 2323
Shapiro MH and Fine J, 1989: J. Nucl. Instrum. Methods **B44**, 43
Shepherd FR, Watson PR, Frost DC, Mitchell KAR, 1978: J. Phys. C. Solid State Phys. **11**, 4591
Sigmund P, 1969: Phys. Rev. **184**, 383
Sigmund P, 1987: Nucl. Instrum. Methods **B27**, 1
Silsbee RH, 1957: J. Appl. Phys. **28**, 1246
Smith R, Harrison Jr DE and Garrison BJ, 1989: Phys. Rev. **B40**, 93
Southern AL, Willis WR and Robinson MT, 1963: J. Appl. Phys. **34**, 3492
Stansfield RA, Broomfield K and Clary D, 1989: Phys. Rev. **B39**, 7680
Szymczak W and Wittmaack K, 1980: Nucl. Instrum. Methods **170**, 341
Thompson MW, 1963: Phys. Lett. **6**, 24
Thompson MW, Reid IH and Farmery BW, 1978: Philos. Mag. **38**, 727
Townes CH, 1944: Phys. Rev. **65**, 310
Tsong IST and Bedrossian P, 1993: Mat. Fys. Medd. Dan. Vid. Selsk. **43**, 209

Van der Veen JF, 1985: Surf. Sci. Rep. **5**, 199
Vicanek M, Jimenez-Rodriguez JJ and Sigmund P, 1989: Nucl. Instrum. Methods **B36**, 124
Von Hippel A, 1926: Ann. Physik **81**, 1043
Wehner GK, 1955: J. Appl. Phys. **26**, 1056
Wehner GK, 1992: private communication relayed to the author aboard the cruise ship Sjælland
Winograd N, 1992: J. Phys. Chem. **96**, 6880
Winograd N and Chang C-C, 1989: Phys. Rev. Lett. **62(21)**, 2568
Winograd N, Baxter JP and Kimock FM, 1982: Chem. Phys. Lett. **88**, 581
Winograd N, Kobrin PH, Schick GA, Baxter JP and Garrison BJ, 1986: Surf. Sci. Lett. **176**, L817
Winograd N, El-Maazawi M, Maboudian R, Postawa Z, Bernardo DN, and Garrison BJ, 1992: J. Chem. Phys. **96**, 6314
Wucher A, Watgen M, Mossner C, Oechsner H and Garrison BJ, 1992: Nucl. Instrum. Methods, **B67**, 531
Xu C, Caffey KP, Burnham JS, Goss SH, Garrison BJ and Winograd N, 1992: Phys. Rev. **B45**, 6776
Yarmoff JA, Cyr DM, Huang JH, Kim S and Williams RS, 1986: Phys. Rev.**B33**, 3856
Young CE, Calaway MF, Pellin MJ and Gruen DM, 1984: J. Vac. Sci. Technol.**A2**, 2782